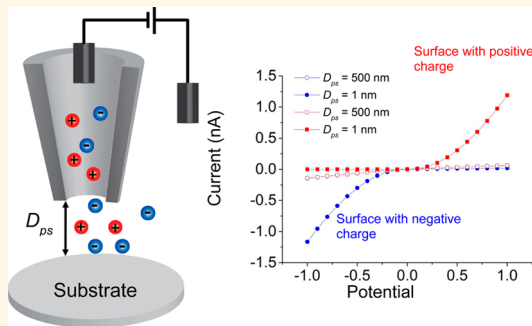


Rectification of Ion Current in Nanopipettes by External Substrates

Niya Sa,^{†,§} Wen-Jie Lan,^{‡,§} Wenqing Shi,[†] and Lane A. Baker^{†,*}

[†]Department of Chemistry, Indiana University, 800 East Kirkwood Avenue, Bloomington, Indiana 47405, United States and [‡]Department of Chemistry, University of Utah, 315 South 1400 East, Salt Lake City, Utah 84112, United States. [§]These authors contributed equally to this work.

ABSTRACT We describe ion distribution and the current–voltage (i – V) response of nanopipettes at different probe-to-substrate distances (D_{ps}) as simulated by finite-element methods. Results suggest electrostatic interactions between a charged substrate and the nanopipette dominate electrophoretic ion transport through the nanopipette when D_{ps} is within 1 order of magnitude of the Debye length (~ 10 nm for a 1 mM solution as employed in the simulation). Ion current rectification (ICR) and permselectivity associated with a neutral or charged nanopipette can be reversibly enhanced or reduced dependent on D_{ps} , charge polarity, and charge density (σ) of the substrate. Regulation of nanopipette current is a consequence of the enrichment or depletion of ions within the nanopipette interior, which influences conductivity of the nanopipette. When the external substrate is less negatively charged than the nanopipette, the substrate first reduces, and then enhances the ICR as D_{ps} decreases. Surprisingly, both experimental and simulated data show that a neutral substrate was also able to reduce and reverse the ICR of a slightly negatively charged nanopipette. Simulated results ascribe such effects to the elimination of ion depletion within the nanopipette at positive potentials.



KEYWORDS: nanopipette · ion current rectification · finite-element simulation · charged interface · Poisson–Nernst–Planck equations

With the development of nanotechnology, nanoscale pipettes (*i.e.*, nanopipettes)^{1–4} have found considerable interest for detection of nanoparticles^{5,6} or single molecules^{7,8} by resistive-pulse approaches, for transduction of analyte binding by changes in current–voltage (i – V) response measurements,^{4,9–13} and for solution-based diode design.^{14,15} A phenomenon observed with nanopipettes and many other nanopores is ion current rectification (ICR), which describes an asymmetric i – V relationship for ion transport. ICR has been explored extensively in both experimental^{2,16–24} and theoretical^{25–34} aspects in recent years. Predominant models suggest enrichment or depletion of counterions at the charged surface of the tip orifice, and an induced asymmetric ionic flux across the nanoscale opening is responsible for ICR.

We have demonstrated previously in experiment that ion current through a nanopipette can be reversibly modified when a nanopipette probe is brought in close

proximity to a charged substrate.²² A comprehensive study, such as the electrostatic effect of surface charge on the ionic current, would benefit from a theoretical understanding of the principles that govern mass transport processes under an imposed external electric field as a nanopipette probe is brought near a charged substrate.

Numerical methods such as finite-element method (FEM) have been utilized extensively to simulate transport processes due to the inherent advantages for solving partial differential equations in complicated or irregular geometries. White and Bund have reported the application of FEM to solve mass transfer problems in nanoscale domains.^{28,35} The accuracy of FEM was verified by solving simple equations with regular geometries (*e.g.*, the electrical double layer at a flat substrate and electroosmosis within a capillary) where known analytical solutions exist. Ion current rectification in a conical-shaped nanopore was simulated with Nernst–Planck, Poisson, and Navier–Stokes equations. Rectification was mainly

* Address correspondence to lanbaker@indiana.edu.

Received for review September 27, 2013 and accepted November 7, 2013.

Published online November 07, 2013
10.1021/nn4050485

© 2013 American Chemical Society

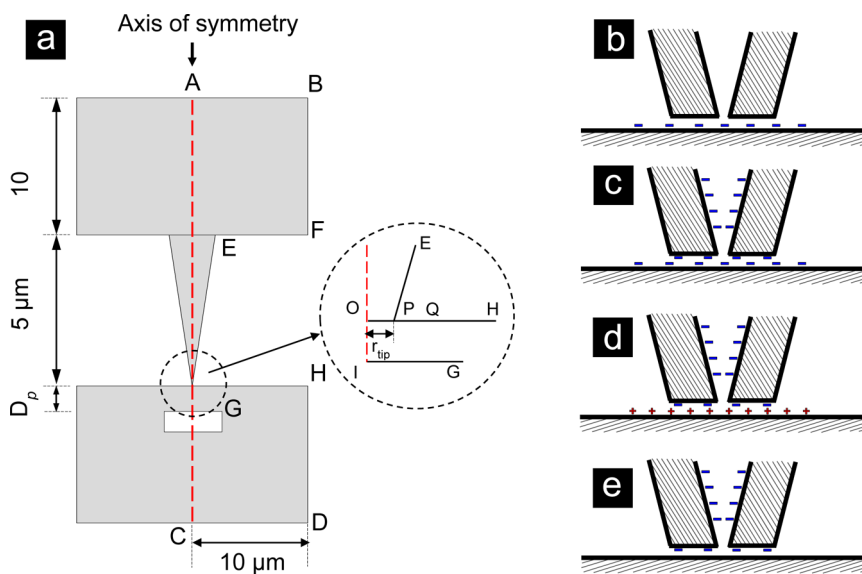


Figure 1. (a) 2D axial symmetric geometry of the nanopipette probe and the substrate used for the finite-element simulations (plot not drawn to scale). Dashed line in red indicates the central probe axis. Detailed definitions for boundary conditions are illustrated in Table S1 in the Supporting Information. The inner diameter (i.d.) and outer diameter (o.d.) of the nanopipette are set as 25 and 200 nm. Ion concentration (C_0) in bulk solution is set to 1 mM. (b–e) Schematic representation of a cross-sectional view for a nanopipette in series with a nanochannel formed between the gap of the nanopipette and substrate at close probe-to-substrate distances: (b) a neutral pipet with a negatively charged substrate, (c) negatively charged pipet and substrate, (d) a negatively charged pipet with a positively charged substrate, and (e) a negatively charged pipet with a neutral substrate.

due to a change in ionic conductivity in the vicinity of the pore orifice at applied bias, which is generated by a redistribution of ions under electric fields from the applied potential and the pore surface charge.

In this paper, we report the simulation of nanopipette probes in close proximity to a charged or neutral substrate with the purpose of understanding the electrostatic interaction at the interface of the probe and substrate (Figure 1a). A systematic study was carried out by alteration of the magnitude and polarity of the surface charge density on either the nanopipette or the external substrate. We found that at short probe-to-substrate distances (D_{ps}), the gap between the nanopipette and substrate can be considered as a nanochannel that is then connected in series to a nanopipette, shown schematically in Figure 1b–e. Surface charge density distributed within this particular T-shape geometry dominates the i – V response at small probe-to-substrate distances (less than 500 nm). Results reported here lead to several findings. First, the local electric field induced by the surface charge of the substrate dominates mass transport at small D_{ps} (less than 500 nm). Second, a neutral substrate can reversibly reduce current rectification in the vicinity of a nanopipette, shown both experimentally and theoretically. Third, and in agreement with previous reports,^{23,28} overlap of the electrical double layers associated with the nanopipette and substrate is not required for manipulation of ion current. The ICR ratio, however, varies significantly when the D_{ps} is less than a few hundred nanometers. Our findings provide an in-depth

understanding of the external-substrate-induced current rectification and mass transfer phenomena within nanoscale domains, and may inform future design of devices for applications in surface recognition and reversible ionic diodes.

RESULTS AND DISCUSSION

For a glass or quartz surface at moderate to high pH, dissociated silanol groups result in negative surface charges, an effect used widely in applications such as capillary electrophoresis,³⁶ contact electrification,³⁷ and studies of ion current rectification.¹ For nanopipettes in particular, surface charge density (σ) plays a critical role in determination of mass transport through the confined geometry at the tip. When a potential is applied across the nanopipette, the large electric field at the nanoscale opening of the pipet results in a unique sensing mechanism that can make use of surface charge.^{27,38–41} Table 1 lists surface charge densities of silica materials reported throughout the literature. Experimental reports of charge density on a flat glass surface or a silica sphere range widely from -10^{-6} to -1.1 e/nm^2 (-10^{-4} to -180 mC/m^2).^{42–45} Surface charge density at the tip region of a nanopipette is not as straightforward as the case of a flat glass surface. Previous simulations utilized σ of -0.001 to -1.5 e/nm^2 (-0.16 to -240 mC/m^2) and produced rectified current responses in good qualitative agreement with measured current–voltage curves.^{2,28,35,46–48} Recent simulations determined σ on a nanopipette wall through fitting experimentally measured i – V curves

TABLE 1. Reported Surface Charge Densities for Silica Materials

material	σ (e/nm ²)	σ (mC/m ²)	note	ref
Silica sphere	$-1.25 \times 10^{-3} \sim -4.38 \times 10^{-3}$	$-0.20 \sim -0.70$	Calculated	42
Glass plate	$-1.25 \times 10^{-3} \sim -3.75 \times 10^{-3}$	$-0.20 \sim -0.60$	Calculated	42
Silica sphere	$-5.5 \times 10^{-4} \sim -8.5 \times 10^{-4}$	$-0.088 \sim -0.14$	Measured	53
PS sphere	$-3.1 \times 10^{-4} \sim -4.4 \times 10^{-3}$	$-0.049 \sim -0.70$	Measured	43
BK7 glass surface	$-0.1875 \sim -1.125$	$-30 \sim -180$	Measured	44
Silica sphere	-0.0005	-0.08	Measured	45
Silica sphere	$-0.013 \sim -0.75$	$-2.1 \sim -120$	Measured	54
Silica sphere	$-1.0 \times 10^{-6} \sim -6.3 \times 10^{-4}$	$-1.6 \times 10^{-4} \sim -0.1$	Measured	55
Oxidized PDMS	-0.08125	-13	Measured	56

with simulated i – V curves and gave σ values from -170 to -240 mC/m².^{47,49} For most simulations, -1 e/nm² (-160 mC/m²) has been used to consider effects of surface charge on current rectification. In addition to surface charge density, pore geometry, electrolyte concentration, and pH are important parameters to consider in simulations of ion current measurement.^{2,48,50} To the best of our knowledge, no direct experimental measurement of surface charge density for a nanopipette exists. For simulations described here, absolute values of σ from 1 to 10 mC/m² are utilized as a compromise between reported values and computational costs of simulation.

Ion Current Rectification of a Neutral Nanopipette Induced by an Externally Charged Substrate ($\sigma_{\text{pipet}} = 0$ mC/m², $\sigma_{\text{sub}} = \pm 1$ mC/m²). In this article, we define the sign of the potential as the potential applied inside of a nanopipette with respect to the potential in the external bulk solution. Current–voltage curves were simulated for a neutral nanopipette brought close to a charged substrate with either negative or positive charge. Figure 2a,b shows simulated i – V curves as D_{ps} varies from 500 to 1 nm. Rectification ratios for each D_{ps} , defined as the current value at -1 V over the current value at $+1$ V, are shown in Figure 2c,d. The neutral nanopipette displays an ohmic response (rectification ratio equals to 1) when D_{ps} is greater than 100 nm at $\sigma_{\text{sub}} = -1$ mC/m². As the nanopipette is moved closer, ion current at positive potential decreases while the absolute value of current at negative potential increases. As a consequence, the current rectification ratio increases as D_{ps} is lowered (Figure 2c). At the shortest distance simulated, $D_{\text{ps}} = 1$ nm, the ICR ratio reaches a value >60 . To understand the origin of this phenomenon, total concentration distributions along the central axis (dashed line, Figure 1a) between the probe and the substrate at ± 1 V are shown in Figure 2e, f for $\sigma_{\text{sub}} = -1$ and $+1$ mC/m². For the case where a neutral nanopipette is close to substrate with $\sigma_{\text{sub}} = -1$ mC/m², with a negative electric potential (inside vs outside) applied across the probe, anions move from the inside of the probe to the external bulk solution. At short probe-substrate distances (e.g., when D_{ps} is 1 nm), the electric field associated with the negative

charge of the substrate is strong enough to occlude anion translocation from nanopipette. This anion rejection leads to a build-up of anion concentration due to the fact that less anions migrate out of the nanopipette at close D_{ps} versus large D_{ps} . Thus, an increase in conductivity of the probe is predicted (Figure 2e, -1 V, $D_{\text{ps}} = 1$ nm). In contrast, with a positive electric potential applied across the probe, anions are depleted from the probe interior while flow of cation toward the probe is inhibited, and this leads to a decrease in the current (Figure 2e, $+1$ V, $D_{\text{ps}} = 1$ nm). Concentration polarization effects, a consequence of local modification of ion concentrations as compared to bulk electrolyte, give rise to greater current rectification (defined as i_{-1V}/i_{+1V}) at small D_{ps} . When the tip is away from the substrate (Figure 2e, ± 1 V, $D_{\text{ps}} = 500$ nm), concentration enrichment observed close to the charged substrate has a negligible effect on the probe conductivity.

Substrate induced current rectification is reversed when the charge of the substrate is changed from -1 mC/m² to $+1$ mC/m² (Figure 2b). Ion current at positive potential increases and ion current at negative potential decreases with reduction of D_{ps} ; therefore, the rectification ratio drops to less than 1 for D_{ps} less than 100 nm (Figure 2d). Simulations for $\sigma_{\text{pipet}} = 0$ mC/m² and $\sigma_{\text{sub}} = \pm 1$ mC/m² suggest that ion current rectification can be influenced by substrate charge. Charge polarity at the substrate dominates ion selectivity at the interface when a neutral nanopipette probe is placed in vicinity of a charged substrate as illustrated in Figure 1b. More pronounced current rectification can also be observed and only requires increase of the surface charge density ($\sigma_{\text{sub}} = -10$ mC/m²), as shown in Figure S1 of the Supporting Information.

Effect of Charge Density of Nanopipette and Substrate. *Surface Charge Density of the Substrate is 10 Times Greater than the Nanopipette ($\sigma_{\text{pipet}} = -1$ mC/m², $\sigma_{\text{sub}} = \pm 10$ mC/m²).* Models in which the substrate has a surface charge density 10 times greater than the probe ($\sigma_{\text{pipet}} = -1$ mC/m², $\sigma_{\text{sub}} = \pm 10$ mC/m²) were examined. Varied surface charge density on the nanopipette or the substrate serves to predict electrostatic effects on ion transport through the nanopipette probe. Figure 1c and 1d illustrate the situation considered in

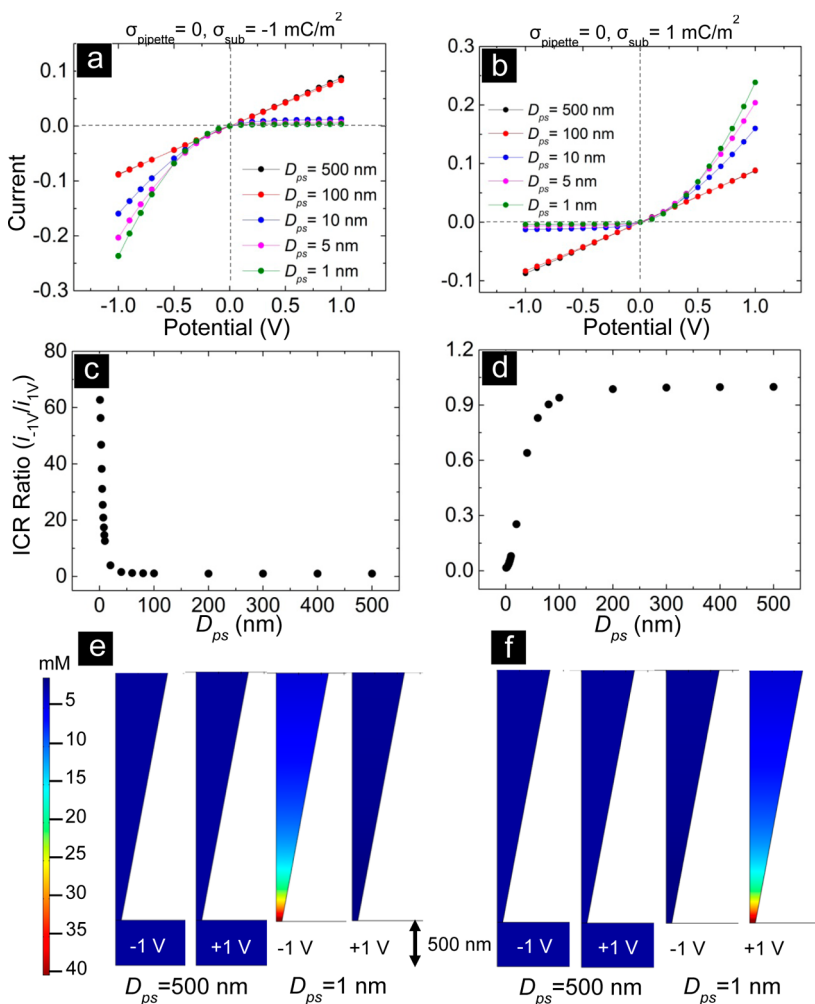


Figure 2. Simulated current–voltage (i – V) curves as a neutral nanopipette ($\sigma_{\text{pipet}} = 0 \text{ mC/m}^2$) approaches (a) a negatively ($\sigma_{\text{sub}} = -1 \text{ mC/m}^2$) and (b) a positively charged substrate ($\sigma_{\text{sub}} = +1 \text{ mC/m}^2$). The corresponding ion current rectification (ICR) ratio is plotted as a function of the distance (D_{ps}) between the probe and the (c) negatively and (d) positively charged substrate. D_{ps} varies from 500 to 1 nm. Simulated total ion concentration distribution at $D_{\text{ps}} = 500$ and 1 nm for (e) $\sigma_{\text{sub}} = -1 \text{ mC/m}^2$ and (f) $\sigma_{\text{sub}} = +1 \text{ mC/m}^2$. The inner diameter (i.d.) and outer diameter (o.d.) of the probe are set as 25 and 200 nm, respectively. The ionic concentration (C_0) in the bulk solution is equal to 1 mM. The ICR ratio is defined as the ratio of the magnitude of the ion current at -1 V relative to that at $+1 \text{ V}$.

this model at close probe-to-substrate distances. Simulated i – V curves and ICR ratios at various D_{ps} for $\sigma_{\text{pipet}} = -1 \text{ mC/m}^2$, $\sigma_{\text{sub}} = \pm 10 \text{ mC/m}^2$ are presented in Figure 3. Similar trends to the case where $\sigma_{\text{pipet}} = 0$ and $\sigma_{\text{sub}} = \pm 1 \text{ mC/m}^2$ are observed, which suggests under these conditions surface charge immobilized on the substrate can dominate ion selectivity at close probe-to-substrate distances despite the existence of the surface charge on the nanopipette. Stronger effects of ion accumulation/depletion result in higher ICR ratios (Figure 3c) when the substrate surface charge is 10 times that of the probe. Concentration distributions along the central axis of the nanopipette (dashed line in Figure 1a) were plotted to understand the origin of this effect. At $D_{\text{ps}} = 500 \text{ nm}$, the charge on the substrate is too far away to exert influence over the ion distribution around the nanopipette (Figure S2, Supporting Information). At $D_{\text{ps}} = 5 \text{ nm}$, negative charges on both the substrate and probe result in ion accumulation at

negative potentials and ion depletion at positive potentials. Moreover, the overall magnitude of the maximum concentration enhancement at $D_{\text{ps}} = 5 \text{ nm}$ increases about 4 times as compared with concentration enhancement at $D_{\text{ps}} = 500 \text{ nm}$. Such concentration enhancement indicates a more polarized concentration profile, which suggests more pronounced ion selectivity arises due to the charged substrate. Contrary to the results for $\sigma_{\text{sub}} = -10 \text{ mC/m}^2$, an increase of ion current carried by cations and anions at positive potentials is predicted at $\sigma_{\text{sub}} = +10 \text{ mC/m}^2$ and rectification drops as D_{ps} decreases (Figure 3d). With these conditions, ions are enriched at positive potentials and depleted at negative potentials as the nanopipette probe approaches the substrate, which results in reversal of i – V response (Figure S2, Supporting Information).

This trend is in good qualitative agreement with experimental reports in which a nanopipette approached a

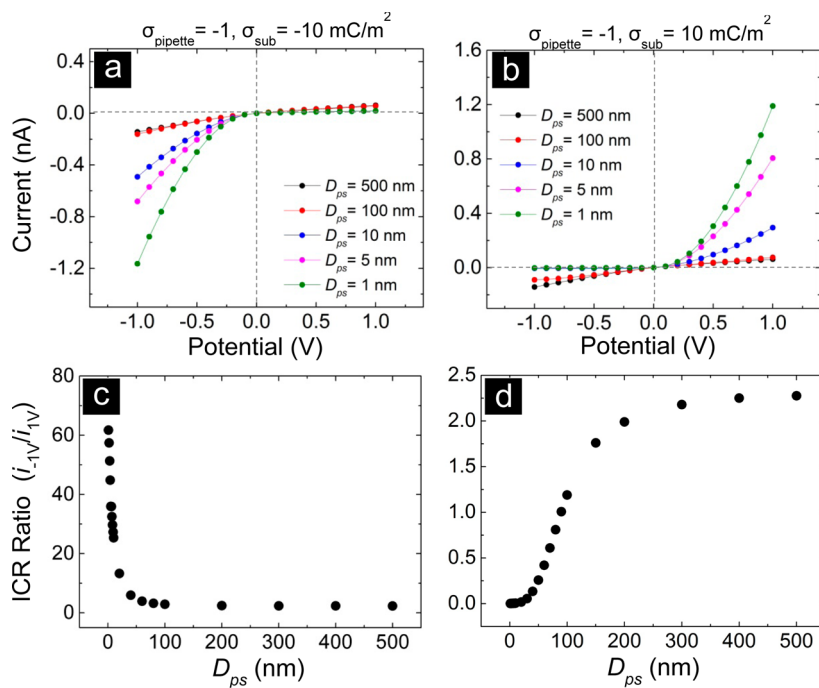


Figure 3. Simulated i – V curves of a negatively charged ($\sigma_{\text{pipet}} = -1 \text{ mC/m}^2$) nanopipette approaching (a) a negatively charged ($\sigma_{\text{sub}} = -10 \text{ mC/m}^2$) substrate and (b) a positively charged substrate ($\sigma_{\text{sub}} = 10 \text{ mC/m}^2$). (c and d) Corresponding plots of the ion current rectification (ICR) ratio as a function of the distance (D_{ps}) between the probe and the substrate. D_{ps} varies from 500 to 1 nm.

PDMS substrate that carries negative or positive charges.²² Results discussed here suggest that substrates with higher charge density (10-fold) can override surface charge effects of the nanopipette alone and can enhance or lower rectification regardless of the presence of surface charge on the nanopipette. As a result, ion selectivity in the gap between the nanopipette probe and substrate is controlled by the charge density at the substrate. We note that the simulation model predicts a counterintuitive current increase at small D_{ps} (<100 nm) and negative (for approaching a negatively charged substrate) or positive potentials (for a positively charged substrate), opposite to previous experimental observation.²² This is possibly due to the difference in electrolyte concentration between the simulation (1 mM) and the experiments (50 mM).

Models Where Surface Charge Density on the Substrate is 10% of That on the Nanopipette ($\sigma_{\text{pipet}} = -10 \text{ mC/m}^2$, $\sigma_{\text{sub}} = \pm 1 \text{ mC/m}^2$). A model with higher σ (-10 mC/m^2) on the nanopipette than on the substrate ($\pm 1 \text{ mC/m}^2$) was examined further to investigate the role of charge density. Current–voltage curves and ICR ratios versus D_{ps} for a model with $\sigma_{\text{pipet}} = -10 \text{ mC/m}^2$, $\sigma_{\text{sub}} = -1 \text{ mC/m}^2$ are presented in Figure 4. As D_{ps} is reduced from 500 to 20 nm, ions accumulate within the probe at negative potentials. However, the charge density on the substrate is lower than that on the probe, which results in a decrease in the ion current at negative potentials and an increase of ion current at positive potentials (Figure 4a). As a consequence, the ICR ratio decreases from 2.0 to 0.8 as D_{ps} is lowered from 500 to 20 nm (Figure 4c). Interestingly, as the

probe continues to approach to the substrate from 20 to 1 nm, the higher electric field adjacent to the substrate induces a decrease in positive currents (Figure 4b), which also results in an increase of the ICR ratio. For instance, the ICR ratio increases from 0.8 to 2.0 as D_{ps} drops from 20 to 1 nm. Concentration distributions are further analyzed to examine correlation of ion distribution to current response. At negative potentials, a concentration polarization zone induced by surface charge on the nanopipette wall exists inside of the nanopipette when the probe is away from the substrate ($D_{\text{ps}} = 500 \text{ nm}$, Figure 4d). At D_{ps} of 20 nm, the magnitude of concentration enhancement appears to be comparable at both positive and negative potentials (Figure 4e). As the probe-to-substrate distance is further decreased to 1 nm, the concentration of ions at negative potentials (64 mM at the tip with a transpipette potential of -1 V) increases significantly and is much higher than at the corresponding positive potential (2.7 mM at 1 V , Figure 4f).

In addition, simulations were performed with reversed charge on the substrate ($\sigma_{\text{pipet}} = -10 \text{ mC/m}^2$, $\sigma_{\text{sub}} = +1 \text{ mC/m}^2$, Figure 5). When the probe is far from the substrate, the asymmetric ion current response is attributed mainly to the surface charge of the probe. As D_{ps} is decreased from 500 to 100 nm, absolute ion current at negative potentials starts to decrease while current at positive potentials remains the same (Figure 5a), similar to the data shown in Figure 4a. The position of maximum concentration enhancement remains inside of the nanopipette orifice; however, the amplitude decreases to 12 mM at $D_{\text{ps}} = 150 \text{ nm}$ as

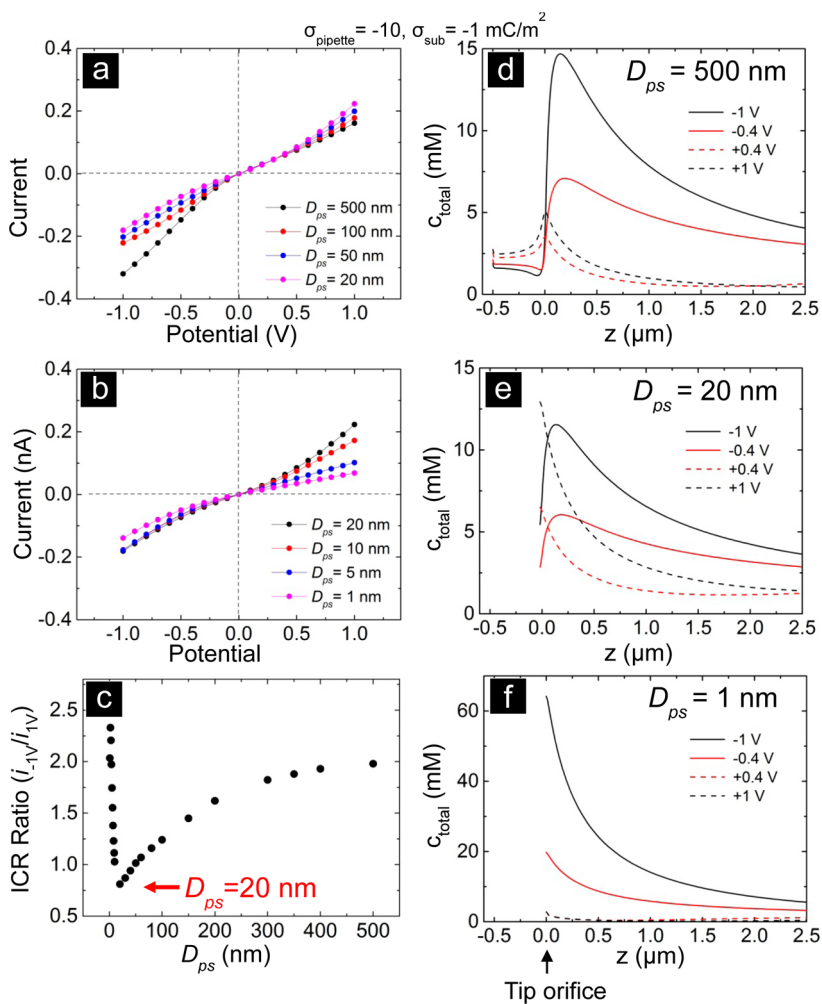


Figure 4. Simulated i – V curves of a negatively charged nanopipette ($\sigma_{\text{pipet}} = -10 \text{ mC/m}^2$) approaching a negatively charged substrate ($\sigma_{\text{sub}} = -1 \text{ mC/m}^2$) from (a) 500 to 20 nm and (b) 20 to 1 nm. (c) Corresponding dependence of ICR ratio vs D_{ps} . (d–f) Simulated total ion concentration distribution as a function of distance along the central probe axis at $D_{ps} = 500$, 20, and 1 nm, respectively.

indicated from Figure 5c (15 mM at $D_{ps} > 500$ nm as shown in Figure 4d). When the probe is closer to the substrate, $D_{ps} = 150$ –1 nm, the positive charge of the substrate controls ion transport through the pore, as suggested by the decrease of current at negative potentials and the increase of current at positive potentials. Thus, the degree of current rectification decreases at lower D_{ps} as shown in Figure 5b. Concentration profiles show a considerable difference at $D_{ps} = 5$ nm compared with $D_{ps} > 150$ nm. At $D_{ps} = 5$ nm, the position of the maximum concentration enhancement shifts closer to the nanopipette orifice. Counterions are built up between the nanopipette probe and the substrate (Figure 5d). Thus, ion distributions are dictated by the surface charge of the substrate at low D_{ps} .

From these simulations, the location of concentration polarization is observed to shift due to the electrostatic interaction of the charged interfaces of nanopipette and substrate. Surface charge on the substrate dominates ion transport when the nanopipette probe is in the vicinity of the surface even if the charge

density on the substrate is 10-fold lower. In addition, our simulations in Figures 4 and 5 suggest that a 100% overlap of the electrical double layers between the probe and the substrate, that is, $D_{ps} < 100$ nm ($\sim 5 \times$ Debye length) for the 1 mM solution used here, is not necessary to effectively change the ICR by the substrate, in agreement with previous studies of ICR phenomena.^{23,28}

Experimental and Simulated Results of ICR of a Negatively Charged Nanopipette in the Presence of a Neutral Substrate ($\sigma_{\text{pipet}} = -1 \text{ mC/m}^2$, $\sigma_{\text{sub}} = 0 \text{ mC/m}^2$). Having established that ICR can be induced by charge from an external substrate, a more complicated situation where a negatively charged nanopipette ($\sigma_{\text{pipet}} = -1 \text{ mC/m}^2$) approaches a neutral substrate is considered ($\sigma_{\text{sub}} = 0 \text{ mC/m}^2$). As the probe is far from the substrate, $D_{ps} = 500$ nm, surface charge immobilized on the nanopipette determines ion selectivity; thus, an asymmetric current–voltage curve is observed with an ICR ratio of ~ 2.3 (Figure 6a,b). The concentration polarization zone is located inside of the nanopipette, ~ 300 nm away

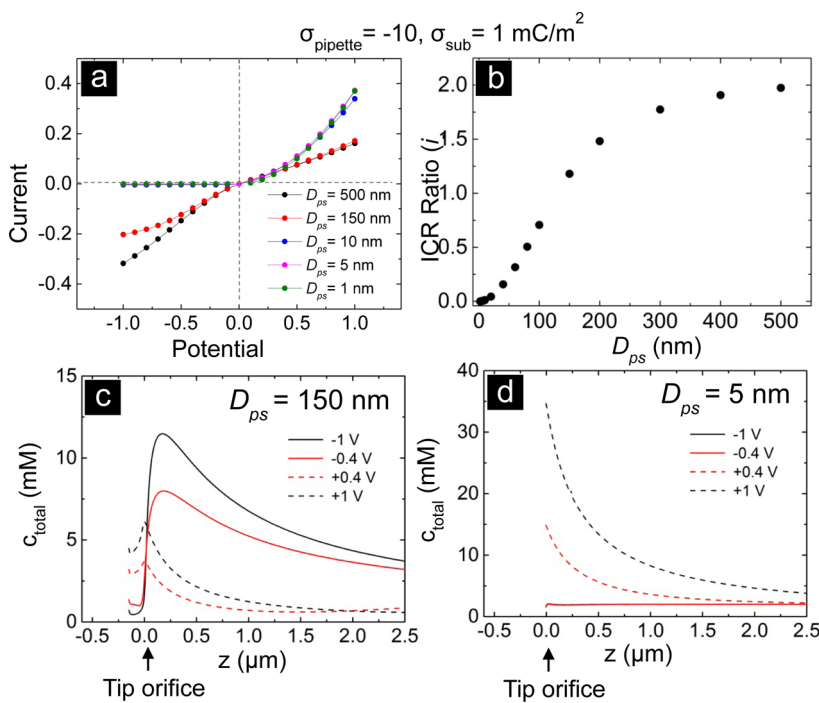


Figure 5. (a) Simulated i - V curves of a negatively charged ($\sigma_{\text{pipette}} = -10 \text{ mC/m}^2$) nanopipette approaching a positively charged ($\sigma_{\text{sub}} = 1 \text{ mC/m}^2$) substrate. (b) Corresponding plot of ICR ratio as a function of the distance (D_{ps}) between the probe and the substrate. D_{ps} varies from 500 to 1 nm. (c and d) Simulated total ion concentration distribution as a function of distance along the central probe axis at $D_{\text{ps}} = 150$ and 5 nm.

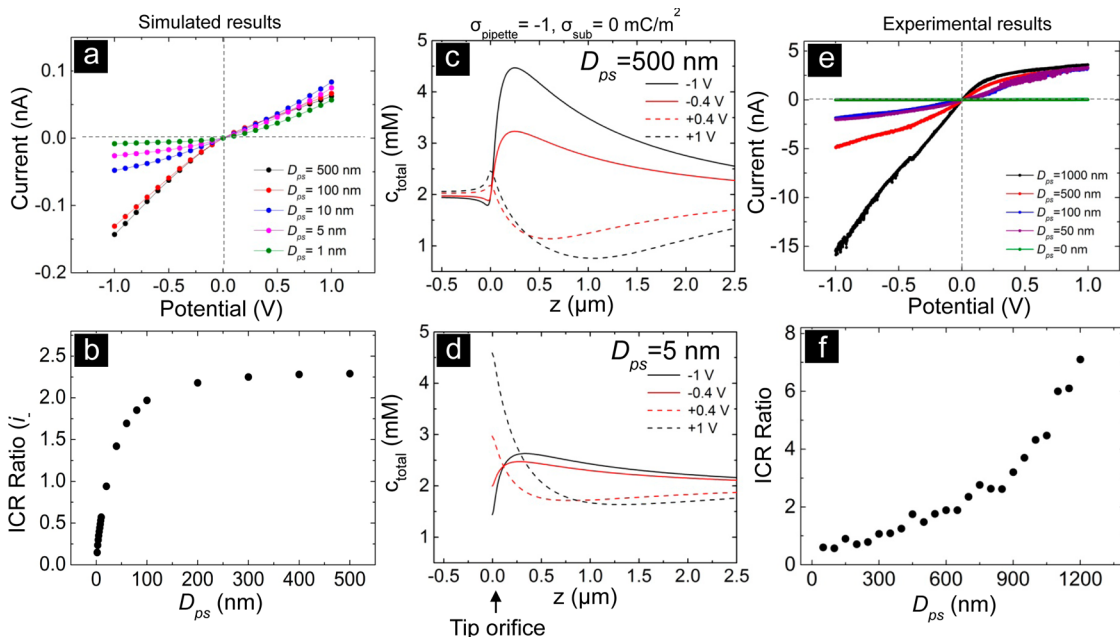


Figure 6. (a) Simulated i - V curves of a negatively charged nanopipette ($\sigma_{\text{pipette}} = -1 \text{ mC/m}^2$) approaching a neutral ($\sigma_{\text{sub}} = 0 \text{ mC/m}^2$) substrate from 500 to 1 nm and (b) corresponding dependence of ICR ratio vs D_{ps} . Simulated total ion concentration distribution as a function of distance along the central probe axis at (c) $D_{\text{ps}} = 500 \text{ nm}$, (d) $D_{\text{ps}} = 5 \text{ nm}$. (e) Experimentally measured i - V curves obtained by approaching a nanopipette probe to a PDMS substrate (model for a neutral surface) and (f) ICR ratio vs D_{ps} . D_{ps} is altered from 1000 to 0 nm. A solution of 50 mM KCl buffered at pH 7.5 is used for both filling electrolyte and the bath solution.

from the tip orifice (Figure 6c), similar to the condition in which the substrate is absent in the system. As D_{ps} is reduced from 500 to 1 nm, the electric field is localized within a confined region of the nanopipette channel in

series with the gap formed at the surface, as illustrated in Figure 1e. In this situation, current at negative potentials is weakly voltage dependent (Figure 6a), especially at low D_{ps} , where ion transport from the bulk

at negative potentials is limited due to the steric hindrance of the substrate. Ion concentration in the pore also becomes less voltage dependent at negative potentials (Figure 6d). At positive potentials, a lack of depletion zone is shown at $D_{ps} = 5$ nm as compared with $D_{ps} = 500$ nm. Ion concentration is depleted to lower than 1 mM at $D_{ps} = 500$ nm (Figure 6c), while the lowest ion concentrations are about 2 mM at $D_{ps} = 5$ nm (Figure 6d). Therefore, no depletion zone is created at positive potentials at close probe-to-substrate distances for a neutral substrate and the existence of the substrate limits current for both voltage polarities. The disappearance of the depletion zone at positive potentials results in the reversal of current rectification ratios at small D_{ps} . Furthermore, a probe with higher charge density, $\sigma_{pipet} = -10$ mC/m², exhibits a similar reduction and reversal of the ICR (Figure S3).

An experiment where a nanopipette is brought toward a nominally neutral PDMS substrate was performed to further investigate this finding. Experimentally, the nanopipette was approached toward a neutral PDMS substrate at D_{ps} ranges from 1200 to 0 nm and i – V curves were recorded at discrete positions. Electrolyte that filled the inside of the nanopipette was identical to the bath electrolyte (50 mM KCl buffered at pH 7.5). Figure 6e and 6f show that experimental measurements are in qualitative agreement with the simulated results where the rectification ratio decreases, primarily due to the current decrease at negative potentials, as the nanopipette probe approaches closer to the substrate. Experimental evidence shows that current–voltage curves are transformed from a rectified response to a quasi-linear response and then into a reversed rectified response. The rectification ratio drops from 7.1 to 1.25 as D_{ps} decreases from 1200 to 400 nm. Current–voltage curves show a linear trend when $D_{ps} = 350$ and 300 nm (ICR = 1.09, 1.07 respectively). Rectification is reversed with reduced D_{ps} and the ICR ratio is 0.8 and 0.6 for $D_{ps} = 250$ and 50 nm, respectively. Similar reproducible experimental results were observed for multiple nanopipettes. Experimental observation of rectification reversal at decreased D_{ps} is in qualitative agreement with the simulated results discussed here. Although finite-element simulations predict the qualitative trend of the experimental D_{ps} dependent rectification ratios for both charged (previously reported)²² and neutral substrates (Figure 6), they do not provide quantitative agreement with experimental observations at different distances. For instance, experimentally determined rectification ratios start to decrease in a more concentrated electrolyte (50 mM) at larger D_{ps} (>1000 nm) as compared with the simulated results (200 nm). In addition, a higher rectification ratio, ICR~8.0, is observed in experiment when the probe is far from the substrate, and thus, the reversal of

rectification requires a larger number of ions to transport and compensate current at negative potentials. We speculate that the low negative surface charge density employed in the simulation, -1 mC/m², together with the time scale of the experimental interrogations of current, may be responsible for the weaker D_{ps} dependence of ICR at larger D_{ps} (>200 nm). Other laboratories also demonstrated that a complicated long ranged surface force interaction between the nanopipette probe and the substrate may also be one of the reasons.⁵⁷

To summarize the above experimental and modeling findings for the case of a charged nanopipette probe close to a neutral substrate, ion selectivity is determined from surface charge on the nanopipette when the probe is far away from the substrate. The presence of an external neutral substrate can overcome electrostatic effects at low D_{ps} values, which gives rise to a reduction of the ICR. We point out this process is totally reversible due to the nature of physical positioning of the nanopipette probe, which has advantages over other methods to study ICR phenomena that make use of a chemical modification of the probe.⁵¹ The above-mentioned discrepancies suggest that a better understanding of the microenvironment between the nanopipette and the substrate, as well as a more sophisticated theoretical model that considers both short-range and long-range charge interactions is required for quantitative prediction of rectification phenomena of channels at the nanoscale.

CONCLUSIONS

In conclusion, finite-element simulations of i – V curves through a nanopipette can successfully predict the previously reported experimental observation of enhanced or diminished ion current rectification when a nanopipette probe is brought close to a negatively or positively charged substrate. When the charge density of the substrate is 10 times higher than that on the probe, the approach of the probe to the substrate leads to an enhanced or reversed current rectification, which depends on the substrate polarity. The slightly charged (± 1 mC/m²) substrate is also capable of transforming i – V curves, but to a lesser extent. Further analysis of the ionic concentration profile suggests that the presence of the adjacent charged substrate shifts the concentration polarization zone and determines the overall current through the probe. Our simulations demonstrate that the full overlap of the electrical double layers associated with the probe and the substrate is not strictly required for the electrostatics to take effect.

Interestingly, we have found—from both experimental and computational data—that current rectification of a charged probe can also be reversed when it is brought toward a neutral substrate, a consequence of hindrance of concentration polarization zone by the neutral substrate.

Simulation of ion transport at charged interface of nanopipette probe and substrate provides a theoretical support to study mass transfer phenomena at nanoscale. These theoretical findings, together with the previously demonstrated feasibility of bringing a probe in proximity

to a substrate with accurately measured probe-to-substrate distance, allow for rational design of nanopipette devices that are capable of measuring localized charge domains, and realization of a nanofluidics-based diode with readily adjustable permselectivity.

EXPERIMENTAL DESIGN AND NUMERICAL MODELS

Experimental Setup and *i*–*V* Characterization. Nanopipettes with typical tip orifice <50 nm were fabricated and mounted on a piezoactuator positioning system as previously reported.²² Electrolyte filled into nanopipette and bath solution is 50 mM KCl buffered with phosphate (conductivity = 6.74 mS/cm), and pH is adjusted to 7.5. Polydimethylsiloxane (PDMS) substrates are prepared through a commercial Sylgard-184 kit (Dow Corning, Midland, MI) without further surface treatment to perform as a neutral substrate. Current–voltage curve measurements are carried out with a CH instrument (CHI910B Electrochemical Analyzer, Austin, TX) with potential ramped from -1.0 V to $+1.0$ V with sample interval of 0.001 V, quiet time is set as 2 s and a relatively low scan rate of 0.1 V/s is applied to ensure the ionic redistribution is faster than the rate of voltage perturbation.²⁰ Approach curves are taken at a constant potential, -1 V, until current magnitude drops to 80% indicating a close probe-to-substrate separation. The nanopipette is positioned toward the substrate by the piezoactuator with 50 nm step size and the corresponding *i*–*V* curve for each step is recorded simultaneously. A gentle contact between the nanopipette and substrate results in formation of a seal between nanopipette and PDMS with evidence of subpicoampere current readout across the potential range. This position is considered to be $D_{ps} = 0$ to calibrate the absolute D_{ps} distances. Finally, the nanopipette is retracted away from the substrate and *i*–*V* is measured and compared with previously obtained *i*–*V* taken before the experiment to ensure the reversibility of the whole process. Approach curves and *i*–*V* curves at each D_{ps} can be found in the Supporting Information (Figures S4 and S5).

Governing Equations. Finite-element method is applied to solve coupled Poisson–Nernst–Planck (PNP) partial differential equations with COMSOL 4.3 Multiphysics (Comsol, Inc.). The Nernst–Planck (N–P) equation (eq 1) describes the ionic transport within a nanopipette including contributions from the diffusion under a concentration gradient (the first term on the right-hand side) and the migration under an electric field (the second term). \mathbf{J}_i , D_i , C_i , and z_i are, respectively, the ion flux vector, the diffusion coefficient, the concentration, and the charge of species i in solution. Φ is the local electric potential, and F , R , and T are the Faraday's constant, the gas constant, and the temperature, respectively. To simplify the calculation, electroosmotic flow in the nanopipette was not considered in the simulation and the system was assumed to be steady-state, eq 2 (also known as continuity equation), in which ∇ is the gradient operator,

$$\mathbf{J}_i = -D_i \nabla C_i - \frac{z_i F}{RT} D_i C_i \nabla \Phi \quad (1)$$

$$\nabla \cdot \mathbf{J}_i = 0 \quad (2)$$

Poisson equation (eq 3) relates the electrostatic potential and electric field with the spatial charge distribution,

$$\nabla^2 \Phi = -\frac{F}{\epsilon \epsilon_0} \sum_i z_i C_i \quad (3)$$

where ϵ_0 and ϵ are the permittivity of the vacuum and relative permittivity of the electrolyte media. The boundary condition of the Poisson equation is presented in eq 4, according to which zero flux is on the nanopipette wall. σ is the surface charge density (C/m^2),

$$\mathbf{n} \cdot \nabla \Phi = -\frac{\sigma}{\epsilon \epsilon_0} \quad (4)$$

The PNP equations were solved simultaneously to yield electric potential and flux distribution profile within the calculation domain. Ionic current (I) was obtained by integrating the total ion flux toward the two semi-infinite boundaries, as shown in eq 5,

$$I = -F \int_s (\mathbf{J}(\text{K}^+) - \mathbf{J}(\text{Cl}^-)) \cdot \mathbf{n} dS \quad (5)$$

where \mathbf{n} , $\mathbf{J}(\text{K}^+)$, $\mathbf{J}(\text{Cl}^-)$, and S stand for the surface normal vector, flux for cation, flux for anion, and the cross-sectional area of the calculation domain, respectively. The dielectric constant of the diluted (1 mM) KCl solution is set as 80; other parameters in the simulation include the diffusion coefficients of K^+ ($1.96 \times 10^{-9} \text{ m}^2/\text{s}$) and Cl^- ($2.03 \times 10^{-9} \text{ m}^2/\text{s}$).⁵²

Definition of Simulation Domain and Boundary Conditions. Figure 1a describes the two-dimensional simulation domain defined in this study. Two $20 \mu\text{m} \times 10 \mu\text{m}$ reservoirs are connected to the base and the tip end of the nanopipette, while an external substrate with defined surface charge density (σ_{sub}) is placed on the tip side of the nanopipette (detailed simulation conditions can be found in the Supporting Information). D_{ps} was defined as the distance between the nanopipette probe and the substrate and was varied between 1 and 500 nm. The inner and outer diameters of the nanopipette are set as 25 and 200 nm, respectively, according to the experimental conditions. The length of the nanopipette probe was $5 \mu\text{m}$. Surface charge densities (σ) on the nanopipette and the substrate are in the range of 0 to $\pm 10 \text{ mC/m}^2$. Electric potentials were applied on the boundaries AB and CD (Figure 1a). The initial concentration for bulk electrolyte is set as 1 mM. The minimum mesh size is set as 0.1 nm with maximum element growth rate as 1.2.

Conflict of Interest: The authors declare no competing financial interest.

Acknowledgment. We gratefully acknowledge funding from National Institutes of Health (NIDDK 1R21DK082990) for the full support of this paper. The author gratefully acknowledges helpful discussion with Professor Zuzanna Siwy from University of California Irvine. W.-J.L. thanks Professor Henry White for support at the University of Utah.

Supporting Information Available: Simulated results for $\sigma_{\text{pipet}} = 0$, $\sigma_{\text{sub}} = -10 \text{ mC/m}^2$; $\sigma_{\text{pipet}} = -1$, $\sigma_{\text{sub}} = \pm 10 \text{ mC/m}^2$ and $\sigma_{\text{pipet}} = -10$, $\sigma_{\text{sub}} = 0 \text{ mC/m}^2$ were shown in Figure S1–S3. Detailed experimental procedure and *i*–*V* curves at different D_{ps} can be found from page S4–S6. Definition of boundary condition is included in Table S1. This material is available free of charge via the Internet at <http://pubs.acs.org>.

REFERENCES AND NOTES

- Wei, C.; Bard, A. J.; Feldberg, S. W. Current Rectification at Quartz Nanopipet Electrodes. *Anal. Chem.* **1997**, *69*, 4627–4633.
- Sa, N.; Baker, L. A. Experiment and Simulation of Ion Transport through Nanopipettes of Well-Defined Conical Geometry. *J. Electrochem. Soc.* **2013**, *160*, H376–H381.
- Morris, C. A.; Friedman, A. K.; Baker, L. A. Applications of Nanopipettes in the Analytical Sciences. *Analyst* **2010**, *135*, 2190–2202.
- Actis, P.; Mak, A.; Pourmand, N. Functionalized Nanopipettes: Toward Label-Free, Single Cell Biosensors. *Bioanal. Rev.* **2010**, *1*, 177–185.
- Lan, W.-J.; Holden, D. A.; Zhang, B.; White, H. S. Nanoparticle Transport in Conical-Shaped Nanopores. *Anal. Chem.* **2011**, *83*, 3840–3847.

6. Lan, W.-J.; Holden, D. A.; Liu, J.; White, H. S. Pressure-Driven Nanoparticle Transport across Glass Membranes Containing a Conical-Shaped Nanopore. *J. Phys. Chem. C* **2011**, *115*, 18445–18452.
7. Bell, N. A. W.; Thacker, V. V.; Hernandez-Ainsa, S.; Fuentes-Perez, M. E.; Moreno-Herrero, F.; Liedl, T.; Keyser, U. F. Multiplexed Ionic Current Sensing with Glass Nanopores. *Lab Chip* **2013**, *13*, 1859–1862.
8. Li, W.; Bell, N. A.; Hernandez-Ainsa, S.; Thacker, V. V.; Thackray, A. M.; Bujdoso, R.; Keyser, U. F. Single Protein Molecule Detection by Glass Nanopores. *ACS Nano* **2013**, *7*, 4129–4134.
9. Fu, Y.; Tokuhisa, H.; Baker, L. A. Nanopore DNA Sensors Based on Dendrimer-Modified Nanopipettes. *Chem. Commun.* **2009**, *4877*–4879.
10. Umehara, S.; Karhanek, M.; Davis, R. W.; Pourmand, N. Label-Free Biosensing with Functionalized Nanopipette Probes. *Proc. Natl. Acad. Sci. U. S. A.* **2009**, *106*, 4611–4616.
11. Sa, N.; Fu, Y.; Baker, L. A. Reversible Cobalt Ion Binding to Imidazole-Modified Nanopipettes. *Anal. Chem.* **2010**, *82*, 9963–9966.
12. Vilozny, B.; Actis, P.; Seger, R. A.; Vallmajó-Martin, Q.; Pourmand, N. Reversible Cation Response with a Protein-Modified Nanopipette. *Anal. Chem.* **2011**, *83*, 6121–6126.
13. Actis, P.; Rogers, A.; Nivala, J.; Vilozny, B.; Seger, R. A.; Jejelowa, O.; Pourmand, N. Reversible Thrombin Detection by Aptamer Functionalized Sting Sensors. *Biosens. Bioelectron.* **2011**, *26*, 4503–4507.
14. Son, D.; Park, S. Y.; Kim, B.; Koh, J. T.; Kim, T. H.; An, S.; Jang, D.; Kim, G. T.; Jhe, W.; Hong, S. Nanoneedle Transistor-Based Sensors for the Selective Detection of Intracellular Calcium Ions. *ACS Nano* **2011**, *5*, 3888–3895.
15. Chen, C.-H.; Lin, C.-T.; Lee, Y.-H.; Liu, K.-K.; Su, C.-Y.; Zhang, W.; Li, L.-J. Electrical Probing of Submicroliter Liquid Using Graphene Strip Transistors Built on a Nanopipette. *Small* **2012**, *8*, 43–46.
16. Siwy, Z.; Gu, Y.; Spohr, H. A.; Baur, D.; Wolf-Reber, A.; Spohr, R.; Apel, P.; Korchev, Y. E. Rectification and Voltage Gating of Ion Currents in a Nanofabricated Pore. *Europhys. Lett.* **2002**, *60*, 349–355.
17. Siwy, Z.; Apel, P.; Dobrev, D.; Neumann, R.; Spohr, R.; Trautmann, C.; Voss, K. Ion Transport through Asymmetric Nanopores Prepared by Ion Track Etching. *Nucl. Instrum. Methods Phys. Res., Sect. B* **2003**, *208*, 143–148.
18. Siwy, Z.; Apel, P.; Baur, D.; Dobrev, D. D.; Korchev, Y. E.; Neumann, R.; Spohr, R.; Trautmann, C.; Voss, K. O. Preparation of Synthetic Nanopores with Transport Properties Analogous to Biological Channels. *Surf. Sci.* **2003**, *532*, 1061–1066.
19. Woermann, D. Electrochemical Transport Properties of a Cone-Shaped Nanopore: High and Low Electrical Conductivity States Depending on the Sign of an Applied Electrical Potential Difference. *Phys. Chem. Chem. Phys.* **2003**, *5*, 1853–1858.
20. Guerrette, J. P.; Zhang, B. Scan-Rate-Dependent Current Rectification of Cone-Shaped Silica Nanopores in Quartz Nanopipettes. *J. Am. Chem. Soc.* **2010**, *132*, 17088–17091.
21. Powell, M. R.; Sa, N.; Davenport, M.; Healy, K.; Vlassiuk, I.; Letant, S. E.; Baker, L. A.; Siwy, Z. S. Noise Properties of Rectifying Nanopores. *J. Phys. Chem. C* **2011**, *115*, 8775–8783.
22. Sa, N.; Baker, L. A. Rectification of Nanopores at Surfaces. *J. Am. Chem. Soc.* **2011**, *133*, 10398–10401.
23. Kovarik, M. L.; Zhou, K.; Jacobson, S. C. Effect of Conical Nanopore Diameter on Ion Current Rectification. *J. Phys. Chem. B* **2009**, *113*, 15960–15966.
24. Lan, W. J.; Holden, D. A.; White, H. S. Pressure-Dependent Ion Current Rectification in Conical-Shaped Glass Nanopores. *J. Am. Chem. Soc.* **2011**, *133*, 13300–13303.
25. Cervera, J.; Schiedt, B.; Ramirez, P. A Poisson/Nernst-Planck Model for Ionic Transport through Synthetic Conical Nanopores. *Europhys. Lett.* **2005**, *71*, 35–41.
26. Cervera, J.; Schiedt, B.; Neumann, R.; Mafe, S.; Ramirez, P. Ionic Conduction, Rectification, and Selectivity in Single Conical Nanopores. *J. Chem. Phys.* **2006**, *124*, 104706.
27. Vlassiuk, I.; Siwy, Z. S. Nanofluidic Diode. *Nano Lett.* **2007**, *7*, 552–556.
28. White, H. S.; Bund, A. Ion Current Rectification at Nanopores in Glass Membranes. *Langmuir* **2008**, *24*, 2212–2218.
29. Kalman, E. B.; Vlassiuk, I.; Siwy, Z. S. Nanofluidic Bipolar Transistors. *Adv. Mater.* **2008**, *20*, 293–297.
30. Ramirez, P.; Apel, P. Y.; Cervera, J.; Mafe, S. Pore Structure and Function of Synthetic Nanopores with Fixed Charges: Tip Shape and Rectification Properties. *Nanotechnology* **2008**, *19*, 315707.
31. Schoch, R. B.; Han, J.; Renaud, P. Transport Phenomena in Nanofluidics. *Rev. Mod. Phys.* **2008**, *80*, 839–883.
32. Vlassiuk, I.; Smirnov, S.; Siwy, Z. Ionic Selectivity of Single Nanochannels. *Nano Lett.* **2008**, *8*, 1978–1985.
33. Davenport, M.; Rodriguez, A.; Shea, K. J.; Siwy, Z. S. Squeezing Ionic Liquids through Nanopores. *Nano Lett.* **2009**, *9*, 2125–2128.
34. Vlassiuk, I.; Smirnov, S.; Siwy, Z. Nanofluidic Ionic Diodes. Comparison of Analytical and Numerical Solutions. *ACS Nano* **2008**, *2*, 1589–1602.
35. White, H. S.; Bund, A. Mechanism of Electrostatic Gating at Conical Glass Nanopore Electrodes. *Langmuir* **2008**, *24*, 12062–12067.
36. Jorgenson, J. W.; Lukacs, K. D. Zone Electrophoresis in Open-Tubular Glass-Capillaries. *Anal. Chem.* **1981**, *53*, 1298–1302.
37. McCarty, L. S.; Whitesides, G. M. Electrostatic Charging Due to Separation of Ions at Interfaces: Contact Electrification of Ionic Electrets. *Angew. Chem., Int. Ed.* **2008**, *47*, 2188–2207.
38. Siwy, Z. S.; Howorka, S. Engineered Voltage-Responsive Nanopores. *Chem. Soc. Rev.* **2010**, *39*, 1115–1132.
39. Cheng, L. J.; Guo, L. J. Nanofluidic Diodes. *Chem. Soc. Rev.* **2010**, *39*, 923–938.
40. Kim, S. J.; Song, Y.-A.; Han, J. Nanofluidic Concentration Devices for Biomolecules Utilizing Ion Concentration Polarization: Theory, Fabrication, and Applications. *Chem. Soc. Rev.* **2010**, *39*, 912–922.
41. Daiguji, H. Ion Transport in Nanofluidic Channels. *Chem. Soc. Rev.* **2010**, *39*, 901–911.
42. Behrens, S. H.; Grier, D. G. The Charge of Glass and Silica Surfaces. *J. Chem. Phys.* **2001**, *115*, 6716–6721.
43. von Grunberg, H. H.; Helden, L.; Leiderer, P.; Bechinger, C. Measurement of Surface Charge Densities on Brownian Particles Using Total Internal Reflection Microscopy. *J. Chem. Phys.* **2001**, *114*, 10094–10104.
44. van Duijvenbode, R. C.; Koper, G. J. M.; Bohmer, M. R. Adsorption of Poly(propylene imine) Dendrimers on Glass. An Interplay between Surface and Particle Properties. *Langmuir* **2000**, *16*, 7713–7719.
45. McCarty, L. S.; Winkelman, A.; Whitesides, G. M. Ionic Electrets: Electrostatic Charging of Surfaces by Transferring Mobile Ions Upon Contact. *J. Am. Chem. Soc.* **2007**, *129*, 4075–4088.
46. Calander, N. Analyte Concentration at the Tip of a Nanopipette. *Anal. Chem.* **2009**, *81*, 8347–8353.
47. Liu, J.; Kvety, M.; Feng, J.; Wang, D.; Wu, B.; Brown, W.; Wang, G. Surface Charge Density Determination of Single Conical Nanopores Based on Normalized Ion Current Rectification. *Langmuir* **2012**, *28*, 1588–1595.
48. Kubeil, C.; Bund, A. The Role of Nanopore Geometry for the Rectification of Ionic Currents. *J. Phys. Chem. C* **2011**, *115*, 7866–7873.
49. Liu, J.; Wang, D.; Kvety, M.; Brown, W.; Li, Y.; Wang, G. Noninvasive Surface Coverage Determination of Chemically Modified Conical Nanopores That Rectify Ion Transport. *Anal. Chem.* **2012**, *84*, 6926–6929.
50. Apel, P. Y.; Blonskaya, I. V.; Orelovitch, O. L.; Ramirez, P.; Sartowska, B. A. Effect of Nanopore Geometry on Ion Current Rectification. *Nanotechnology* **2011**, *22*, 175302.
51. He, Y.; Gillespie, D.; Boda, D.; Vlassiuk, I.; Eisenberg, R. S.; Siwy, Z. S. Tuning Transport Properties of Nanofluidic Devices with Local Charge Inversion. *J. Am. Chem. Soc.* **2009**, *131*, 5194–5202.

52. Hille, B. *Ion Channels of Excitable Membranes*, 3rd ed.; Sinauer Associates, Inc.: Sunderland, MA, 2001.
53. Behrens, S. H.; Grier, D. G. Pair Interaction of Charged Colloidal Spheres near a Charged Wall. *Phys. Rev. E* **2001**, *64*, 050401.
54. Sonnenfeld, J. Surface Charge Density on Spherical Silica Particles in Aqueous Alkali Chloride Solutions. *Colloid Polym. Sci.* **1995**, *273*, 932–938.
55. Yamanaka, J.; Hayashi, Y.; Ise, N.; Yamaguchi, T. Control of the Surface Charge Density of Colloidal Silica by Sodium Hydroxide in Salt-Free and Low-Salt Dispersions. *Phys. Rev. E* **1997**, *55*, 3028–3036.
56. Duffy, D. C.; McDonald, J. C.; Schueller, O. J. A.; Whitesides, G. M. Rapid Prototyping of Microfluidic Systems in Poly(dimethylsiloxane). *Anal. Chem.* **1998**, *70*, 4974–4984.
57. Clarke, R. W.; Zhukov, A.; Richards, O.; Johnson, N.; Ostanin, V.; Klenerman, D. Pipette-surface Interaction: Current Enhancement and Intrinsic Force. *J. Am. Chem. Soc.* **2013**, *135*, 322–329.